JOURNAL OF GEOPHYSICAL RESEARCH, VOL. ???, XXXX, DOI:10.1029/,

Analysis of thermospheric response to magnetospheric inputs

Yue Deng, Astrid Maute, Arthur D. Richmond and Ray R. Roble

High Altitude Observatory, National Center for the Atmospheric Research,
Boulder Colorado, U.S.A.

Yue Deng (e-mail: ydeng@ucar.edu), Astrid Maute (e-mail: maute@ucar.edu), Arthur D. Richmond (e-mail: richmond@ucar.edu), Ray G. Roble (e-mail: roble@ucar.edu).

Abstract.

Coupling a new empirical model of the Poynting flux with the NCAR-TIEGCM, the influence of the high-latitude energy inputs and heating distributions on the global thermosphere are investigated. First, in order to show the contribution of the electric field variability to the energy input and thermospheric temperature, model results are compared for simulations where Joule heating is calculated with the average electric field (called ”simple Joule heating”) and where Joule heating is adjusted according to the Poynting flux from the empirical model. In the northern (summer) hemisphere, the Poynting flux has a peak in the dayside cusp, which is missing in the altitude-integrated simple Joule heating. The hemispheric integral of the Poynting flux is approximately 30% larger than the integral of simple Joule heating, and the polar average (poleward of $40°$) temperature calculated with the Poynting flux increases by 85-95 K, which is more than 50% of the temperature increase caused by the polar energy inputs. Second, three different methods to distribute the Poynting flux in altitude are investigated. Different heating distributions cause a difference in the polar average of heating per unit mass as high as 40% at 160 km altitude. Consequently, the difference of the polar average temperature among these three cases is close to 30-50 K. These results suggest that not only the total amount of energy input, but the way to distribute the energy in altitude is significant to the impact of the magnetosphere on the thermosphere and ionosphere.

1. Introduction

Electric fields and currents associated with magnetosphere-ionosphere interactions, along with auroral particle precipitation, are important sources of thermospheric energy and momentum, affecting the global thermospheric temperature, density, composition, and winds [e.g., *Volland*, 1979; *Fuller-Rowell and Rees*, 1980, 1981; *Roble et al.* 1982; *Fuller-Rowell et al.*, 1987,1997; *Rees and Ruller-Rowell*, 1989; *Crowley et al.*, 1989; *Mikkelsen and Larsen*, 1991; *Rees*, 1995; *Rishbeth and Müller-Wodarg*, 1999; *Immel et al.*, 2001]. The effects are strongest during and following magnetic storms, but also influence the quiet thermosphere. To develop first-principle thermospheric models with forecast capabilities therefore requires accurate information about the magnetospheric inputs. Although global general-circulation models are able to reproduce the general features of thermospheric responses to magnetospheric inputs, the quantitative application of these models for predictive purposes is limited by uncertainties in the intensities and distributions of the inputs. This limitation applies not only to thermospheric general circulation models (TGCMs) used for analyses of thermospheric variability, like the National Center for Atmospheric Research (NCAR) Thermosphere-Ionosphere-Electrodynamics General-Circulation Model (TIE-GCM) [*Roble et al.*, 1988; *Richmond et al.*, 1992], the Coupled Thermosphere-Ionosphere-Plasmasphere model (CTIP) [*Millward et al.*, 2001] and Global Ionosphere-Thermosphere model (GITM) [*Ridley et al.*, 2006], but also to climatological models that include coupling to the lower atmosphere, like the NCAR Thermosphere-Ionosphere-Mesosphere-Electrodynamics General-Circulation Model [*Roble and Ridley*, 1994] and the NCAR Whole Atmosphere Community Climate Model (WACCM) [*Garcia et al.*, 2007].

Joule heating per unit volume, q_J, can be calculated from the relation

$$q_J = \sigma_P(\mathbf{E} + \mathbf{u}_n \times \mathbf{B})^2$$

$$= \rho\lambda_P(\mathbf{E} \times \mathbf{B}/B^2 - \mathbf{u}_{n\perp})^2 \quad (1)$$

$$\lambda_P = \sigma_P B^2/\rho \quad (2)$$

where σ_P is the Pedersen conductivity, λ_P is the Pedersen ion-drag coefficient, **E** is the electric field, **B** is the magnetic field, $\mathbf{u}_n$ is the neutral wind velocity, $\mathbf{u}_{n\perp}$ is its component perpendicular to **B**, and ρ is the neutral density. The Joule heating rate is related to the total electromagnetic energy transfer rate to the thermosphere, $\mathbf{J} \cdot \mathbf{E}$ (where **J** is the electric current density), by

$$\mathbf{J} \cdot \mathbf{E} = q_J + \mathbf{u}_{n\perp} \cdot \mathbf{J} \times \mathbf{B} \quad (3)$$

[e.g., *Lu et al.*, 1995; *Thayer et al.*, 1995; *Fujii et al.*, 1999]. The last term in (3) represents the rate of work done by the Ampère force on the wind. For time scales longer than a minute or so, the electromagnetic energy transfer rate equals the convergence of the perturbation Poynting vector (or Poynting flux) **S**:

$$\mathbf{J} \cdot \mathbf{E} = -\nabla \cdot \mathbf{S}. \quad (4)$$

$$\mathbf{S} = \mathbf{E} \times \mathbf{\Delta B}/\mu_0 \quad (5)$$

where $\Delta\mathbf{B}$ is the magnetic perturbation due to ionospheric and field-aligned currents and μ_0 is the permeability of free space. If (4) is integrated over the entire volume of ionospheric regions where **J** has a component parallel to **E** (essentially those regions of significant Pedersen conductivity), and if Gauss' theorem is applied, it is found that the integral of the downward component of **S** over the top of the ionosphere, S_{down}, equals the volume integral of $\mathbf{J} \cdot \mathbf{E}$, since the integral of the upward component of **S** over the bottom of the ionosphere vanishes. In fact, it is often a good approximation to relate the *local* value of $S_{\rm down}$ at the top of the ionosphere to the height integral of $\mathbf{J}\cdot\mathbf{E}$ [e.g., *Kelley et al.*, 1991]. *Gary et al.* [1994, 1995] have summarized observations of $S_{\rm down}$ from Dynamics Explorer-2 (DE-2) spacecraft data. *Lu et al.* [1995] and *Thayer et al.* [1995], using TGCM simulations, have shown that the height integrals of $\mathbf{J}\cdot\mathbf{E}$ and of q_J tend to be comparable, although positive or negative differences on the order of 25% can exist. When further integrated horizontally [*Lu et al.*, 1995], the two quantities were found to have very similar values. That is, in an average sense the net amount of electromagnetic energy transfer to the kinetic energy of the wind (the last term in (3)) is usually only a small fraction of the Joule heating and the local value of $S_{\rm down}$ approximately equals to the height integral of Joule heating. (We should note that estimates by *Fujii et al.* [1999] from EISCAT radar measurements found a considerable fraction of $\mathbf{J}\cdot\mathbf{E}$ going into $\mathbf{u}_n\cdot\mathbf{J}\times\mathbf{B}$ on the average. However, the estimation of $\mathbf{u}_n\cdot\mathbf{J}\times\mathbf{B}$ from radar data is sensitive to the assumed model of ion-neutral collision frequency, and so this result should be treated with caution.)

Empirical models have been developed to characterize the auroral precipitation [e.g., *Hardy et al.*, 1987, 1991; *Fuller-Rowell and Evans*, 1987; *Sharber et al.*, 2000] and high-latitude electric potential [e.g., *Foster et al.*, 1986; *Ruohoniemi and Greenwald*, 1996; *Ridley et al.*, 2000; *Weimer*, 2001] under various geophysical conditions. These empirical models are often used to force TGCMs. However, the models of the electric potential represent only the statistical average of the vector field $\mathbf{E}$, $\langle\mathbf{E}\rangle$. The difference between $\mathbf{E}$ and $\langle\mathbf{E}\rangle$,

$$\mathbf{E}' = \mathbf{E} - \langle\mathbf{E}\rangle \qquad (6)$$

is not negligible. For the purposes of the present work, we call $\mathbf{E}'$ the "residual electric field." *Codrescu et al.* [1995] pointed out that $\mathbf{E}'$ might contribute significantly to the total thermospheric Joule heating, because of the non-linear dependence of the heating on the electric field. Indeed, *Codrescu et al.* [2000], *Crowley and Hackert* [2001], and *Matsuo et al.* [2003] showed that the mean square of $\mathbf{E}'$, $\langle \mathbf{E}'^2 \rangle$ can be comparable to or even larger than the square of the mean $\mathbf{E}$, $\langle \mathbf{E} \rangle^{\mathbf{2}}$. It is expected that $\mathbf{E}'$ varies considerably more rapidly than $\langle \mathbf{E} \rangle$, and in a rather random fashion, so that it will tend to be uncorrelated with $\mathbf{u}_n$, and the Poynting flux associated with it will therefore tend to go nearly entirely into Joule heating. Some modeling studies [e.g., *Emery et al.*, 1999] have attempted to account for the additional heating by multiplying the calculated Joule heating by a substantial factor, sometimes as large as 2.5, in order to obtain thermospheric responses that are reasonably consistent with observations. Because of the importance of the residual electric field on Joule heating, there is a need to quantify the Joule heating associated with it in a way consistent with the empirical model of electric potential used as TGCM inputs. In this paper, the Joule heating is specified two ways: one way, either calculated from the average electric field, or specified by the Poynting flux from an empirical model based on the Dynamics Explorer 2 (DE-2) satellite data. The difference between them indicates the contribution from the residual electric field.

Because the thermosphere and ionosphere do not necessary respond in a linear fashion to the high-latitude energy inputs, certain aspects of their response can be quite sensitive to the intensity and distribution of the inputs. For example, the boundary between midlatitude regions where the O/N_2 densities are increased or decreased during a storm, which strongly influences the boundary between regions of positive and negative ionospheric storm effects, depends on the intensity of high-latitude heating, with consequent upwelling and equatorward transport of molecular-rich air [e.g., *Richmond and Lu*, 2000]. Another nonlinear effect we will discuss further in the next section concerns the thermospheric response to distribution of the Joule heating. Concentrated heating can lead to significantly greater net upwelling of molecular species than the same amount of total heating spread over a larger area [*Smith*, 2000]. In this study, three different ways to distribute the Poynting flux in altitude are compared to emphasize the response of thermosphere to the distribution of energy inputs.

2. Model description and simulation conditions

2.1. Poynting flux empirical model

A comprehensive, mutually consistent set of models of high-latitude thermospheric forcing is developed by analyzing observations of electric and magnetic fields and ion drift velocities from the DE-2 spacecraft, and will be detailed in a separate publication. An empirical model of the downward Poynting flux S_{down} at the top of the thermosphere is developed using the combined ion-drift and magnetometer data. The observations are fitted, at each magnetic latitude, to analytical functions of magnetic local time (MLT), dipole tilt angle with respect to the plane normal to the Sun-Earth line, and strength and clock angle of the B_y and B_z components of the interplanetary magnetic field (IMF).

Empirical models of the electric potential and of the horizontal component of $\triangle B$ above the ionosphere are constructed from the DE-2 RPA/IDM and MAGB data, and parameterized in terms of the same parameters as the model of S_{down}, in order to have a mutually consistent set of models. *Weimer* [2001] used the DE-2 VEFI electric-field data to construct an empirical model of high-latitude electric potential, representing large-scale electric fields. *Matsuo et al.* [2003] fitted the potential to the DE-2 RPA/IDM data, with results generally consistent with the *Weimer* model [*Weimer* 2005] except for larger potentials at equinox when the IMF B_z is negative.

2.2. TIEGCM

The thermosphere general circulation model (TGCM) [*Dickinson et al.*, 1981, 1984] is a global circulation model that was developed at the National Center for Atmospheric Research (NCAR) in the early 80's. It calculates the properties of the upper atmosphere, such as the temperature, composition and wind velocity. The Thermosphere Ionosphere-GCM (TIGCM) [*Roble et al.*, 1988] includes a self-consistent ionosphere, and Thermosphere Ionosphere Electrodynamic-GCM (TIEGCM) [*Richmond et al.*, 1992] is an extension of this model that incorporates electrodynamic processes. The TIEGCM simulates self-consistently the neutral winds, conductivities, electric fields and currents. The model also calculates the neutral gas temperature and mass mixing ratios of $O_2, N_2, O, N(^2D), N(^4S)$ and NO. It also solves the electron and ion temperatures and the number densities of O^+, O_2^+, NO^+, N_2^+ and N^+. The model has $5°$ longitude by $5°$ latitude by $1/2$ scale height resolution. The vertical coordinate has 29 constant pressure levels from approximately 97 km to 500 km altitude. At the lower boundary (97 km), the model is forced by tidal perturbations. Below $60°$ magnitude latitude the electric field is calculated by solving the electrodynamo equations, and above $60°$ latitude an electric potential pattern is imposed to describe the electric field.

2.3. Simulation conditions

The high-latitude forcing in the TIEGCM can be specified in different ways, and so there will be different ways in which the empirical high latitude driver models can be used to help specify the forcing. One mode of TIEGCM forcing is to use empirical climatological models of the forcing, varying in time according to the variations of the geophysical parameters used as inputs to the empirical model (e.g., day of year, UT, and K_p). In this paper, the newly developed empirical models provide the required high-latitude forcing: electric potential and downward Poynting flux at the top of thermosphere.

Four TIEGCM runs are compared, which are called the ”simple Joule heating” case, the ”Poynting-Joule” case, the ”Poynting-Pedersen” case and the ”Poynting-Diff” case, respectively. For all of the cases, IMF $B_z = -10nT$, $F_{10.7} = 150 \times 10^{-22} W/m^2/Hz$ and the hemispheric power (HP) is 16 GW. The simulated day number is 181, when the northern hemisphere is in the summer and the southern hemisphere is in the winter. The differences among these runs are the energy inputs in the high latitudes and the way to distribute the energy inputs in altitude. For the ”simple Joule heating” case, the TIEGCM is driven by the average electric potential pattern from the empirical model and the energy input is the simple Joule heating, which is calculated with the average electric field ($q_e = q_{simple} = \sigma_p(\langle \mathbf{E} \rangle + \mathbf{u_n} \times \mathbf{B})^2$). For the ”Poynting-Joule” case, the Poynting flux is assumed to be equal to the height-integrated Joule heating. The Poynting flux is then distributed in altitude proportionally to the calculated simple Joule heating ($q_e = \frac{q_{simple}}{\int_h q_{simple} dh} S_{down}$), and used in place of the previously calculated simple Joule heating. For the ”Poynting-Pedersen” case, it is the same as the ”Poynting-Joule” case except the Poynting flux is distributed in altitude according the Pedersen conductivity ($q_e = \frac{\sigma_p}{\int_h \sigma_p dh} S_{down}$). For the ”Poynting-Diff” case, the altitude integrated simple Joule heating and the Poynting flux from the empirical model are compared. When the Poynting flux is larger than the altitude integrated simple Joule heating, the difference between them is then distributed in altitude according the Pedersen conductivity ($q_e = q_{simple} + \frac{\sigma_p}{\int_h \sigma_p dh}(S_{down} - \int_h q_{simple} dh)$); otherwise, the simple Joule heating is reduced by the ratio of the Poynting flux to the altitude integrated simple Joule heating ($q_e = q_{simple} \frac{S_{down}}{\int_h q_{simple} dh)}$), in order to avoid the possibility of large negative heating at certain locations. The energy inputs and the distribution methods are summarized in the table 1.

Table 1 : Energy inputs and altitude distribution methods

Case	Simple JH	Poynting-Joule	Poynting-Pedersen	Poynting-Diff
Energy input	simple JH	Poynting	Poynting	Poynting
Alt-distribute	NA	simple JH	Pedersen conductivity	difference according Pedersen

3. Results

3.1. Energy inputs specified by simple Joule heating and Poynting flux

In GCMs, simple Joule heating is internally computed according to the GCM's algorithms, based on the smoothed electric field, neutral wind and conductivity. The empirical model of the Poynting flux gives the magnitude of the Poynting flux, which is then assumed to be equal to the height-integrated Joule heating. Figure 1 shows the net electromagnetic energy flux from the magnetosphere into the thermosphere, with the altitude-integrated simple Joule heating on the left side and the Poynting flux from the empirical model on the right side. It is clear that they have different distributions as well as different magnitudes. In the northern (summer) hemisphere, the altitude-integrated simple Joule heating maximizes on the dawn and dusk sides, while the Poynting flux has an additional peak in the noon-time cusp region. In the southern (winter) hemisphere, the altitude-integrated simple Joule heating has a larger maximum value on the duskside, and the Poynting flux has a more even distribution between dawnside and duskside. In addition, the summer-winter difference is larger in the Poynting flux than in the altitude integrated simple Joule heating. The large maximum of the Poynting flux at local noon in the northern (summer) hemisphere is seasonally dependent and reduced significantly in the winter. The total energy input (288 GW + 236 GW) for the Poynting flux case is 30% larger than the simple Joule heating case (207 GW + 190 GW). In the empirical model, the Poynting flux is computed using point measurements of the electric field and magnetic field, not the smoothed fields, and shows the total electromagnetic energy input from the magnetosphere. On the other hand, the simple Joule heating is calculated using the average electric field, which does not include small-scale variations. Thus, this 30% difference indicates the contribution of the electric field and conductivity variability to the total energy input. In this paper, we concentrate on the electric field variation assuming that the contribution of the small-scale conductivity variation is negligible. Since the Poynting flux has a more apparent cusp region peak in the northern (summer) hemisphere than the southern (winter) hemisphere, the following discussion concentrates on the northern (summer) hemisphere.

the Poynting flux from the empirical model represents the energy flux at the top of thermosphere, which has a two dimensional distribution. In order to get a three dimensional profile of the energy inputs, it is necessary to distribute the Poynting flux in altitude. In the polar region, the magnetic field is almost vertical and the magnetic field lines are equipotentials, and it is reasonable to assume that electric field and magnetic field change little with altitude. If the neutral wind is ignored, the altitude distribution of Joule heating only depends on the Pedersen conductivity, and distributing the Poynting flux in height according the Pedersen conductivity is very straightforward. After this expansion, the horizontal distribution of the heating per unit mass in the northern (summer) hemisphere at a particular altitude (400 km), shown in Figure 2, is similar to the distribution of the total energy flux at the top of thermosphere, shown in Figure 1. However, since the Pedersen conductivity is not uniform in space, the two distributions are not identical. For example, in the northern (summer) hemisphere, where the Poynting flux on the dawnside has a comparable magnitude as on the duskside, as shown on the right of Figure 1(A), the heating per unit mass on the duskside at 400 km altitude, shown in the middle of Figure 2, is much larger than that on the dawnside.

Figure 3 shows the vertical wind distributions for the simple Joule heating case, Poynting flux case and the difference between them. The maximum vertical velocity is close to 10 m/s, which is relatively small compared with the horizontal velocity. In general, the vertical wind is upward on the dayside and downward on the nightside. The maximum upward wind and the maximum downward wind are separated by the day-night terminator. The vertical wind difference, shown on the right of Figure 3, shows a strong correlation with the heating difference, shown on the right of Figure 2. For example, the duskside maximum in the heating difference corresponds to a maximum in the upward neutral velocity difference, while the dawnside minimum in the heating difference corresponds to the minimum in the vertical velocity difference. Due to the complexity of the advection, the response of the vertical neutral velocity to the energy input is not linear. For example, while the difference heating in the cusp is smaller than that at dusk, the cusp difference neutral wind actually is larger than that on the duskside. Also, the peak positions do not totally overlap. The region of negative heating difference extends to later local times than does the negative wind difference, which is shifted toward the nightside by several hours.

Figure 4 represents the thermosphere-ionosphere response in the northern (summer) hemisphere when the energy inputs are specified by the simple Joule heating and by the Poynting flux. As shown in Figure 4(A), the temperature distributions for the simple Joule heating and the Poynting flux cases have similar structures, with higher temperatures in the afternoon sector than in the morning sector below 60° latitude. The difference of Poynting flux case from the simple Joule heating case is in the right column, which shows the temperature increases in the whole polar region with a maximum of more than 100 K. There are three temperature difference peaks, in the late-morning sector, on the dusk side, and around midnight. Interestingly, the temperature difference does not correspond to the heating difference very well. This is because the temperature is under the influence of several mechanisms, including adiabatic cooling, thermal conductivity and advection, as well as heating. While there is no positive heating difference in Figure 2 at midnight, there is a positive neutral temperature difference peak in Figure 4 (A) around midnight at 60° latitude. This neutral temperature increase is possibly correlated with the downward neutral wind difference, shown in Figure 3 (B), which results in an adiabatic heating. The increased temperature brings more N_2 to high altitudes, and thus the O/N_2 ratio difference exhibits a negative correlation with the temperature difference. As shown in Figure 4, on the duskside, where there is a peak in the temperature difference, the O/N_2 ratio decreases by more than 0.7 (around 40%) and creates a small green negative region. At 400 km altitude, where diffusion is more important than chemical reactions to the electron density, a rough correlation between the differences of the O/N_2 ratio and electron density can be seen in Figure 4. The electron density decreases in most places where the O/N_2 ratio difference is negative. The distributions show that both the O/N_2 ratio and the electron density decrease more on the dusk side than on the dawn side.

Figure 5 displays the altitude profiles of the polar average (poleward of 40° for the northern hemisphere and poleward of -40° for the southern hemisphere) heating per unit mass. At most altitudes, the heating per unit mass in the Poynting flux case is larger than that in the simple Joule heating case. Also, the summer-winter difference is greater for the Poynting flux case (red lines) than the simple Joule heating case (black lines). Below 300 km altitude, the larger summer-winter difference in Poynting flux case is partially due to the 20% greater total energy input in the summer hemisphere. As a consequence of the hemispherically symmetric distributions of electric field and particle precipitation in the empirical models, there is almost no summer-winter difference for the simple Joule heating at low altitudes. Above 300 km, interestingly, the heating per unit mass in the winter hemisphere (dot lines) is larger than that in the summer hemisphere (solid lines). The explanation is that in response to the seasonal neutral composition change, winter F-region electron densities and thus Pedersen conductivities are generally larger in winter than in summer.

The polar average neutral temperature for both the simple Joule heating and the Poynting flux cases are shown in Figure 6. Using the Poynting flux leads to an 85 K temperature increase in the southern (winter) and 95 K increase in the northern (summer) hemisphere, as compared with the simple Joule heating case. In order to show wether these 85-95 K temperature increases are significant or not, we made another run without Joule heating. As shown in Figure 6, compared with the simple Joule heating case (black lines), the temperature decreases by 160 K (125 K) in the southern (northern) hemisphere when there is no Joule heating (green lines). Therefore, those 85-95 K temperature increases are more than 50% of the temperature changes caused by the polar energy inputs.

3.2. Impact of the Poynting flux distribution

When the average electric field and residual electric field are described separately, the Joule heating can be written as:

$$q_J = \sigma_p(\langle \mathbf{E} \rangle + \mathbf{E}' + \mathbf{u_n} \times \mathbf{B})^{\mathbf{2}} \tag{7}$$

$$q_J = \sigma_p(\langle \mathbf{E} \rangle + \mathbf{u_n} \times \mathbf{B})^{\mathbf{2}} + 2\sigma_p \mathbf{E}' \cdot (\langle \mathbf{E} \rangle + \mathbf{u_n} \times \mathbf{B}) + \sigma_p \mathbf{E}'^{\mathbf{2}} \tag{8}$$

In the ”Poynting-Pedersen” case, which is discussed in section 3.1, the Poynting flux is assumed to equal to the altitude integrated Joule heating and the energy inputs are distributed proportionally to the Pedersen conductivity. The assumption in this method is that the average electric field ($\langle \mathbf{E} \rangle$), electric field variation ($\mathbf{E}'$) and neutral wind ($\mathbf{u_n}$) change little in altitude. Therefore, the energy input is proportional to the Pedersen conductivity. Two other methods are also investigated in this study: one way is to distribute the Poynting flux in height proportionally to the simple Joule heating calculated with the average electric field ($\sigma_p(\langle \mathbf{E} \rangle + \mathbf{u_n} \times \mathbf{B})^{\mathbf{2}}$). This method, called ”Poynting-Joule”, assumes that $\mathbf{E}' \propto (\langle \mathbf{E} \rangle + \mathbf{u_n} \times \mathbf{B})$, which implies that the neutral winds respond to the change of ion drag force very quickly and totally follow the electric field variation. The other way, named ”Poynting-Diff”, is to distribute the difference between the Poynting flux and the altitude-integrated simple Joule heating in altitude according to the Pedersen conductivity in regions where the Poynting flux is larger than the altitude-integrated simple Joule heating. For places where the Poynting flux is smaller than the altitude-integrated simple Joule heating, the simple Joule heating is reduced by a certain ratio to make the altitude-integrated Joule heating equal to the Poynting flux. In this way, it is assumed that the neutral wind does not respond to the electric field variation at all and the residual electric field, $\mathbf{E}'$, is not correlated with the average electric field $\langle \mathbf{E} \rangle$. The second term in equation (8) vanishes (on the average), and the difference between the Poynting flux and the altitude-integrated simple Joule heating is the third term in equation (8). This difference is proportional to σ_p, since $\mathbf{E}'$ changes little with altitude. From the assumptions of the three methods, it seems that the ”Poynting-Diff” is the most reasonable way to distribute the Poynting flux, since the neutral wind is not constant in altitude, nor does it respond to the electric field variation very rapidly. But in order to the evaluate the different methods, they need to be compared with observations to test which way matches the known features of thermospheric variability best.

Figure 7 shows the heating per unit mass at 400 km altitude for the three different ways to distribute the Poynting flux in altitude. Interestingly, the three cases have different altitude distributions of heating, while they have exactly the same energy inputs at the top of thermosphere. While the ”Poynting-Joule” case has a maximum value on the dawn side, the ”Poynting-Pedersen” distribution has more significant maxima in the cusp region and on the dusk side, and the ”Poynting-Diff” has a similar distribution as the ”Poynting-Pedersen” case, except that the dawn cell is enhanced.

In order to investigate the impact of the energy distributions on the thermosphere, the difference of each case from the background case (simple Joule heating) is shown in Figure 8, including the difference distributions of the heating per unit mass, vertical wind and temperature with respect to the simple Joule heating case. The vertical wind difference shows a strong influence from the heating difference, and basically, where there is a positive (negative) heating difference, there is an upward (downward) vertical wind. Because the heating difference is not the only forcing for the vertical wind difference, there are some other vertical wind difference peaks without corresponding heating difference peaks, such as the upward wind difference close to 02 LT around 60° latitude in the ”Poynting-Pedersen” case. Figure 8 (C) shows that the ”Poynting-Joule” case has the smallest temperature variations and the ”Poynting-Pedersen” case has the largest. There is a persistent temperature increase maximum around 9-13 LT in the morning sector below 60° latitude, which is possibly caused by the variation of horizontal and vertical convection. The position of the second temperature difference peak varies from case to case. The ”Poynting-Joule” case maximizes in the early morning sector around 60° latitude, but the ”Poynting-Pedersen” case has a maximum on the dusk side, which is related to the maximum Poynting flux on the dusk side, as shown in Figure 8 (A). The ”Poynting-Diff” case has a similar distribution as the ”Poynting-Pedersen” case, except that the magnitude is reduced. The distribution of the temperature difference does not correspond to the heating difference very well, which is due to the contribution of other mechanisms, such as adiabatic cooling, thermal conductivity and advection, as mentioned in the previous section.

As shown in Figure 9 (A), the polar average heating per unit mass in the northern (summer) hemisphere in the ”Poynting-Joule” case (blue line) is smaller than in the ”Poynting-Diff” case (green line) and ”Poynting-Pedersen” case (red line) above 120 km altitude, while the total energy inputs from magnetosphere are the same. At 160 km altitude, the ”Poynting-Joule” is 40% smaller than ”Poynting-Pedersen”, which is caused by the differences in altitude distribution of energy associated primarily with wind effects. As shown in Figure 9 (B), more energy is distributed below 120 km altitude in the ”Poynting-Joule” case than in the ”Poynting-Pedersen” case, and the absolute value of the heating difference is larger below 120 km altitude than above 120 km. However, due to the exponential decrease of mass density with height, the difference of heating per unit mass above 120 km is more significant. Figure 10 shows that all cases using the Poynting flux to specify the energy input have a consistent enhancement of the polar average neutral temperature compared with the simple Joule heating case, and the increased amplitude in the northern hemisphere varies from 40 to 95 K depending on the way to distribute the Poynting flux in altitude. This result indicates not only the total energy input, but also the distribution of energy can make some difference to the thermospheric response to the magnetospheric inputs.

4. Conclusion and discussion

A new set of quantitative empirical models of the high-latitude forcing of the thermosphere, including electric potential and Poynting flux, are used with the NCAR-TIEGCM to investigate the influence of the high-latitude forcing on the neutral temperature, composition and electron density.

First, the simple Joule heating calculated with the average electric field and the Poynting flux from the empirical model are compared to show the contribution of electric field variability to the Joule heating. The total energy of the Poynting flux is close to 30% larger than the integrated simple Joule heating. In the northern (summer) hemisphere, the Poynting flux has an apparent cusp peak, which is missing in the altitude-integrated simple Joule heating. Due to the non-uniform distribution of the conductivity, the distribution of heating per unit mass at 400 km altitude is different from the distribution of total energy flux at the top of thermosphere. In general, the vertical wind difference between the Poynting flux case and the simple Joule heating case is upward (downward) where the heating per unit mass difference is positive (negative). The neutral temperature in the Poynting flux case increases in the whole polar region compared with the simple Joule heating case and the increased magnitude can reach 100 K. The distribution of temperature difference does not correspond very well to the distribution of heating difference, because other mechanisms, such as adiabatic cooling, thermal conductivity and advection, are important to the temperature as well as the energy source. The decreased O/N_2 ratio shows an inverse relationship with the temperature change, and leads to an electron density reduction in almost the whole polar region. The polar average temperature increases by 85-95 K, which is more than 50% of the temperature change caused by the polar energy inputs.

Secondly, the inter-comparison among three different methods to distribute the Poynting flux in altitude is conducted. The increase of the heating per unit mass, compared with the simple Joule heating case at 400 km altitude, has different distributions and magnitudes for the three cases. The resulting maximum increase of the temperature varies from 60 to 135 K. Due to the differences in altitude distribution of heating, the polar average of the heating per unit mass for the ”Poynting-Joule” case can be 40% smaller than the ”Poynting-Pedersen” case around 160 km altitude, while these two cases have the same amount of the total energy input from the magnetosphere. The corresponding difference of the polar average temperature between these two cases is close to 50 K in the northern hemisphere. This result suggests that not only the total amount of energy input, but the way to distribute the energy are important to the impact of magnetospheric forcing on the thermosphere and ionosphere.

Acknowledgments.

This research was supported by NSF through grants *** and NASA grant ***.

The editor thanks both of the referees for their assistance in evaluating this paper.

References

Codrescu, M.V., T.J. Fuller-Rowell, and J.C. Foster, On the importance of E-field variability for Joule heating in the high-latitude thermosphere, *Geophys. Res. Lett.*, *22*, 2393-2396, 1995.

Codrescu, M.V., T.J. Fuller-Rowell, J.C. Foster, J.M. Holt, and S.J. Cariglia, Electric field variability associated with the Millstone Hill electric field model, *J. Geophys. Res.*, *105*, 5265-5273, 2000.

Crowley, G., and C.L. Hackert, Quantification of high latitude electric field variability, *Geophys. Res. Lett.*, *28*, 2783-2786, 2001.

Crowley, G., B. A. Emery, R. G. Roble, H. C. Carlson, Jr., and D. J. Knipp, Thermospheric dynamics during September 18-19, 1984, 1. Model simulations, *J. Geophys. Res.*, *94*, 16,925-16,944, 1989.

Dickinson, R. E., E. C. Ridley, and R. G. Roble, A three-dimensional time-dependent general circulation model of the thermosphere, *J. Geophys. Res., 86*, 1499, 1981.

Dickinson, R. E., E. C. Ridley, and R. G. Roble, Thermospheric general circulation with coupled dynamics and composition, *J. Atmos. Solar-Terr. Phys., 41*, 205, 1984.

Emery, B.A., C. Lathuillere, P.G. Richards, R.G. Roble, M.J. Buonsanto, D.J. Knipp, P. Wilkinson, D.P. Sipler, and R. Niciejewski, Time dependent thermospheric neutral response to the 2-11 November 1993 storm period, *J. Atmos. Solar-Terr. Phys., 61*, 329-350, 1999.

Foster, J.C., J.M. Holt, R.G. Musgrove, and D.S. Evans, Ionospheric convection associated with discrete levels of particle precipitation, *Geophys. Res. Lett., 13*, 656-659, 1986.

Fujii, R., S. Nozawa, S.C. Buchert, and A. Brekke, Statistical characteristics of electromagnetic energy transfer between the magnetosphere, the ionosphere, and the thermosphere, *J. Geophys. Res., 104*, 2357-2365, 1999.

Fuller-Rowell, T., and Evans, D. S., Height-integrated Pedersen and Hall conductivity patterns inferred from the TIROS-NOAA satellite data, *J. Geophys. Res.*, 92, 7606-7618, 1987.

Fuller-Rowell, T., and D. Rees, A three-dimensional time-dependent global model of the thermosphere, *J. Atmos. Sci., 37*, 2545-2567, 1980.

Fuller-Rowell, T.J., and D. Rees, A three-dimensional time-dependent simulation of the global dynamical response of the thermosphere to a geomagnetic substorm, *J. Atmos. Terr. Phys., 43*, 701-721, 1981.

Fuller-Rowell, T.J., S. Quegan, D. Rees, R.J. Moffett, and G.J. Bailey, Interactions between neutral thermospheric composition and the polar ionosphere using a coupled ionosphere-thermosphere model, *J. Geophys, Res., 92*, 7744-7748, 1987.

Fuller-Rowell, T.J., M.V. Codrescu, B.G. Fejer, W. Borer, F. Marcos, and D.N. Anderson, Dynamics of the low-latitude thermosphere: quiet and disturbed conditions, J. Atmos. Solar-Terr. Phys., 59, 1533-1540, 1997.

Gary, J. B., R. A. Heelis, W. B. Hanson, and J. A. Slavin, Field-aligned Poynting flux observations in the high-latitude ionosphere, *J. Geophys. Res.*, *99*, 11417-11427, 1994.

Gary, J.B., R.A. Heelis, and J.P. Thayer, Summary of field-aligned Poynting flux observations from DE2, *Geophys. Res. Lett.*, *22*, 1861-1864, 1995.

Garcia, R. R., D. R. Marsh, D. E. Kinnison, B. A. Boville, and F. Sassi, Simulation of secular trends in the middle atmosphere, 1950-2003, *J. Geophys. Res.*, *112*, 9301-+, 2007.

Hardy, D.A., M.S. Gussenhoven, R. Raistrick, and W.J. McNeil, Statistical and functional representations of the pattern of auroral energy flux, number flux, and conductivity, *J. Geophys. Res.*, *92*, 12,275-12,294, 1987.

Hardy, D.A., W. McNeil, M.S. Gussenhoven, and D. Brautigam, A statistical model of auroral ion precipitation, 2. Functional representation of the average pattern, *J. Geophys. Res.*, *96*, 5539-5547, 1991.

Immel, T.J., G. Crowley, J.D. Craven, and R.G. Roble, Dayside enhancements of thermospheric O/N_2 following magnetic storm onset, *J. Geophys. Res.*, *106*, 15,471-15,488, 2001.

Kelley, M.C., D.J. Knudsen, and J.F. Vickrey, Poynting flux measurements on a satellite: a diagnostic tool for space research, *J. Geophys. Res.*, *96*, 201-207, 1991.

Lu, G., A.D. Richmond, B.A. Emery, and R.G. Roble, Magnetosphere-ionosphere-thermosphere coupling: effect of neutral wind on energy transfer and field-aligned current, *J. Geophys. Res.*, *100*, 19,643-19,659, 1995.

Matsuo, T., *Effects of high-latitude ionospheric electric field variability on the estimation of global thermospheric Joule heating*, Ph.D. thesis, State University of New York at Stony Brook, 2003.

Matsuo, T., A.D. Richmond, and D.W. Nychka, Modes of high-latitude electric field variability derived from DE-2 measurements: Empirical Orthogonal Function (EOF) analysis, *Geophys. Res. Lett., 29*(7), 1107, doi:10.1029/2001GL014077, 2002.

Matsuo, T., A. D. Richmond, and K. Hensel, High-latitude ionospheric electric field variability and electric potential derived from DE-2 plasma drift measurements: Dependence on IMF and dipole tilt, *J. Geophys. Res., 108*(A1), 1005, doi:10.1029/2002JA009429, 2003.

Mikkelsen, I.S., and M.F. Larsen, A numerical modeling study of the interaction between the tides and the circulation forced by high-latitude plasma convection, *J. Geophys. Res., 96*, 1203-1213, 1991.

Millward, G.H., A.D. Aylward, I.C.F. Mueller-Wodarg, T.J. Fuller-Rowell, R.J. Moffett, and A.D. Richmond, An investigation into the influence of tidal forcing on F region equatorial vertical ion drift using a global ionosphere-thermosphere model with coupled electrodynamics, *J. Geophys. Res., 106*, 24,733-24,744, 2001.

Rees, D., Observations and modelling of ionospheric and thermospheric disturbances during major geomagnetic storms: a review, *J. Atmos. Terr. Phys., 57*, 1433-1457, 1995.

Rees, D., and T.J. Fuller-Rowell, The response of the thermosphere and ionosphere to magnetospheric forcing, *Phil. Trans. Roy. Soc. London, A328*, 139-171, 1989.

Richmond, A.D., Assimilative mapping of ionospheric electrodynamics, *Adv. Space Res., 12*, (6)59-(6)68, 1992.

Richmond, A.D., Ionospheric electrodynamics using Magnetic Apex Coordinates, *J. Geomagn. Geoelectr., 47*, 191-212, 1995.

Richmond, A.D., and G. Lu, Upper-atmospheric effects of magnetic storms: a brief tutorial, *J. Atmos. Solar-Terr. Phys., 62*, 1115-1127, 2000.

Richmond, A.D., and J.P. Thayer, Ionospheric electrodynamics: a tutorial, in *Magnetospheric Current Systems*, edited by R.L. Lysak, M. Hesse, R. Fujii, and S. Ohtani, pp. 131-146, Am. Geophys. Union, Washington, D.C., 2000.

Richmond, A.D., E.C. Ridley, and R.G. Roble, A thermosphere/ionosphere general circulation model with coupled electrodynamics, *Geophys. Res. Lett., 19*, 601-604, 1992.

Ridley, A.J., G. Crowley, and C. Freitas, An empirical model of the ionospheric electric potential, *Geophys. Res. Lett., 27*, 3675-3678, 2000.

Ridley, A. J., Y. Deng, and G. Toth, The global ionosphere-thermosphere model, *J. Atmos. Sol-Terr. Phys., 68*, 839, 2006.

Rishbeth, H., and I.C.F. Müller-Wodarg, Vertical circulation and thermospheric composition: a modelling study, *Ann Geophysicae, 17*, 794-805, 1999.

Roble, R.G., and E.C. Ridley, A thermosphere-ionosphere-mesosphere-electrodynamics general circulation model (time-GCM): equinox solar cycle minimum simulations (30-500 km), *Geophys. Res. Lett., 21*, 417-420, 1994.

Roble, R.G., R.E. Dickinson, and E.C. Ridley, Global circulation and temperature structure of thermosphere with high-latitude plasma convection, *J. Geophys. Res., 87*, 1599-1614, 1982.

Ruohoniemi, J.M., and R.A. Greenwald, Statistical patterns of high-latitude convection obtained from Goose Bay HF radar observations, *J. Geophys. Res., 101*, 21,743-21,763, 1996.

Sharber, J.R., J.D. Winningham, R.A. Frahm, G. Crowley, A.J. Ridley, and R. Link, Empirical modeling of particle precipitation and the study of effects on the terrestrial thermosphere and ionosphere, *Phys. Chem. Earth C*, *25* 489-493, 2000.

Smith, R.W., The global-scale effect of small-scale thermospheric disturbances, *J. Atmos. Solar-Terr. Phys.*, *62*, 1623-1628, 2000.

Thayer, J.P., J.F. Vickrey, R.A. Heelis, and J.B. Gary, Interpretation and modeling of the high-latitude electromagnetic energy flux, *J. Geophys. Res.*, *100*, 19,715-19,728, 1995.

Volland, H., Magnetospheric electric fields and currents and their influence on large scale thermospheric circulation and composition, *J. Atmos. Solar-Terr. Phys.*, *41*, 853-866, 1979.

Weimer, D.R., An improved model of ionospheric electric potentials including substorm perturbations and application to the Geospace Environment Modeling November 24, 1996, event, *J. Geophys. Res.*, *106*, 407-416, 2001.

Weimer, D.R., Improved ionospheric eletrodynamic models and application to calculating Joule heating rates, *J. Geophys. Res.*, *110*, 5306-+, 2005.

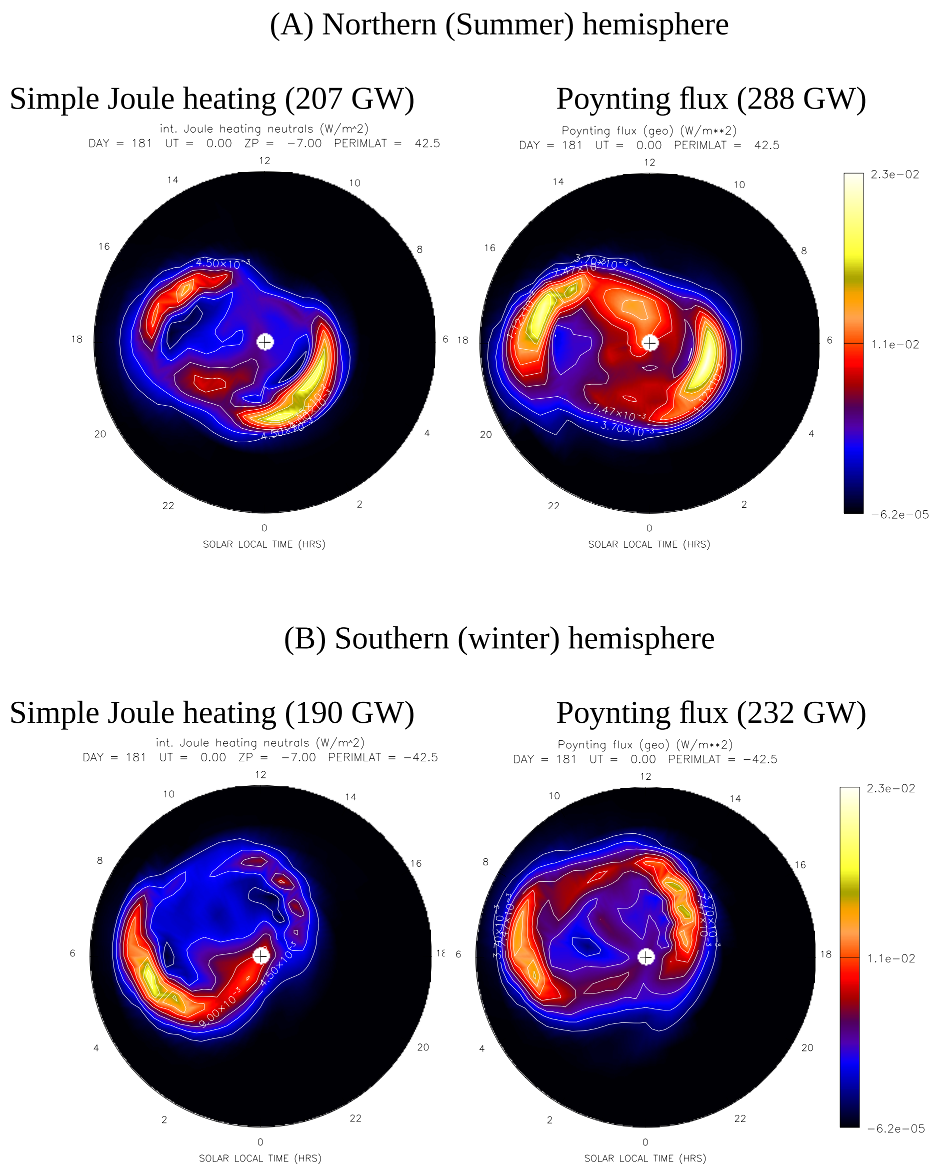

Figure 1. Total energy flux (W/m^2) at the top of thermosphere from the magnetosphere for the (A) northern (summer) hemisphere and (B) southern (winter) hemisphere on DOY=181. The left column shows the altitude-integrated simple Joule heating and the right column shows the Poynting flux from the empirical model. The total energy is shown in brackets in the title. The outside ring is $42.5°$ geographic latitude for the northern hemisphere and $-42.5°$ for the southern hemisphere. All of the polar distributions in this paper are plotted in geographic coordinates.

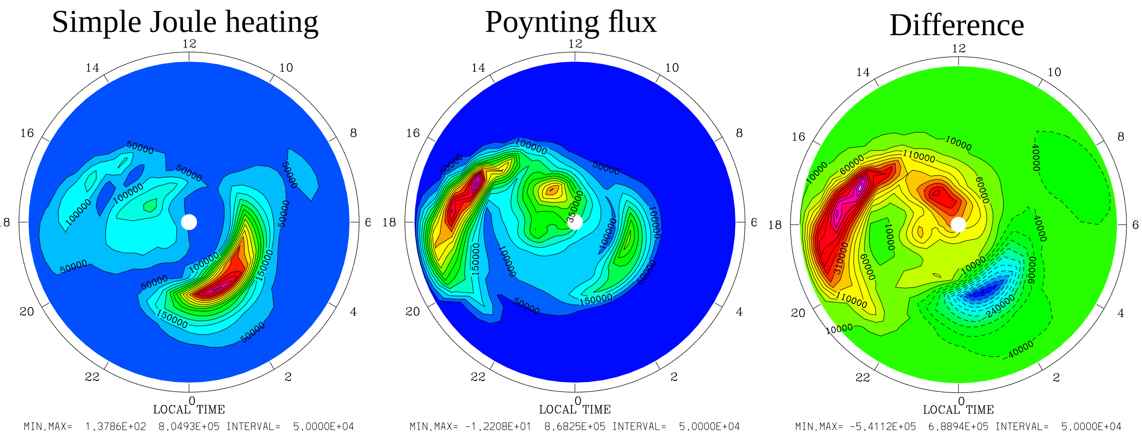

Figure 2. Heating per unit mass ($erg/g/s[= 10^{-4}W/kg]$) at 400 km altitude in the northern (summer) hemisphere for (Left) the simple Joule heating case, (Middle) the Poynting flux case and (Right) the difference between these two cases. Note that the difference distribution has different scale than the heating distributions.

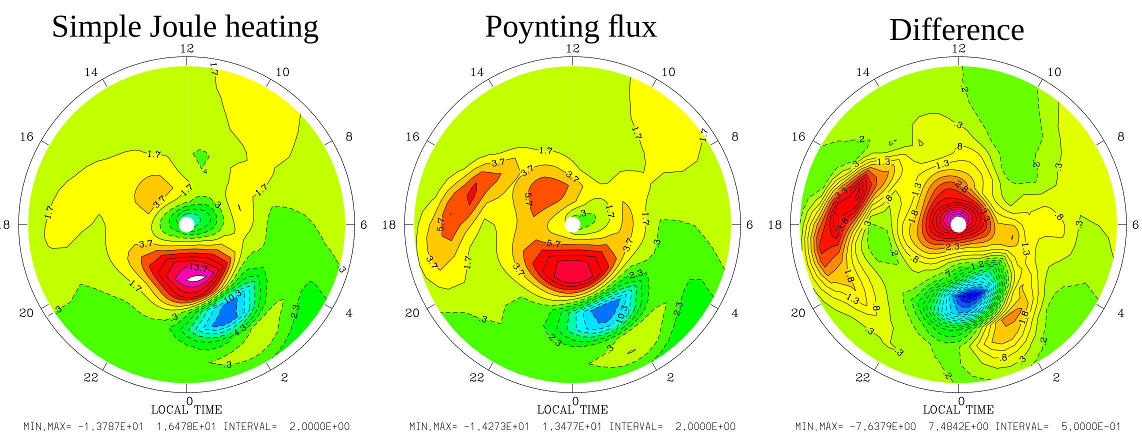

Figure 3. Same as Figure 2, but for vertical neutral wind (m/s). Note that the scale for the difference velocity is amplified by a factor of 2.

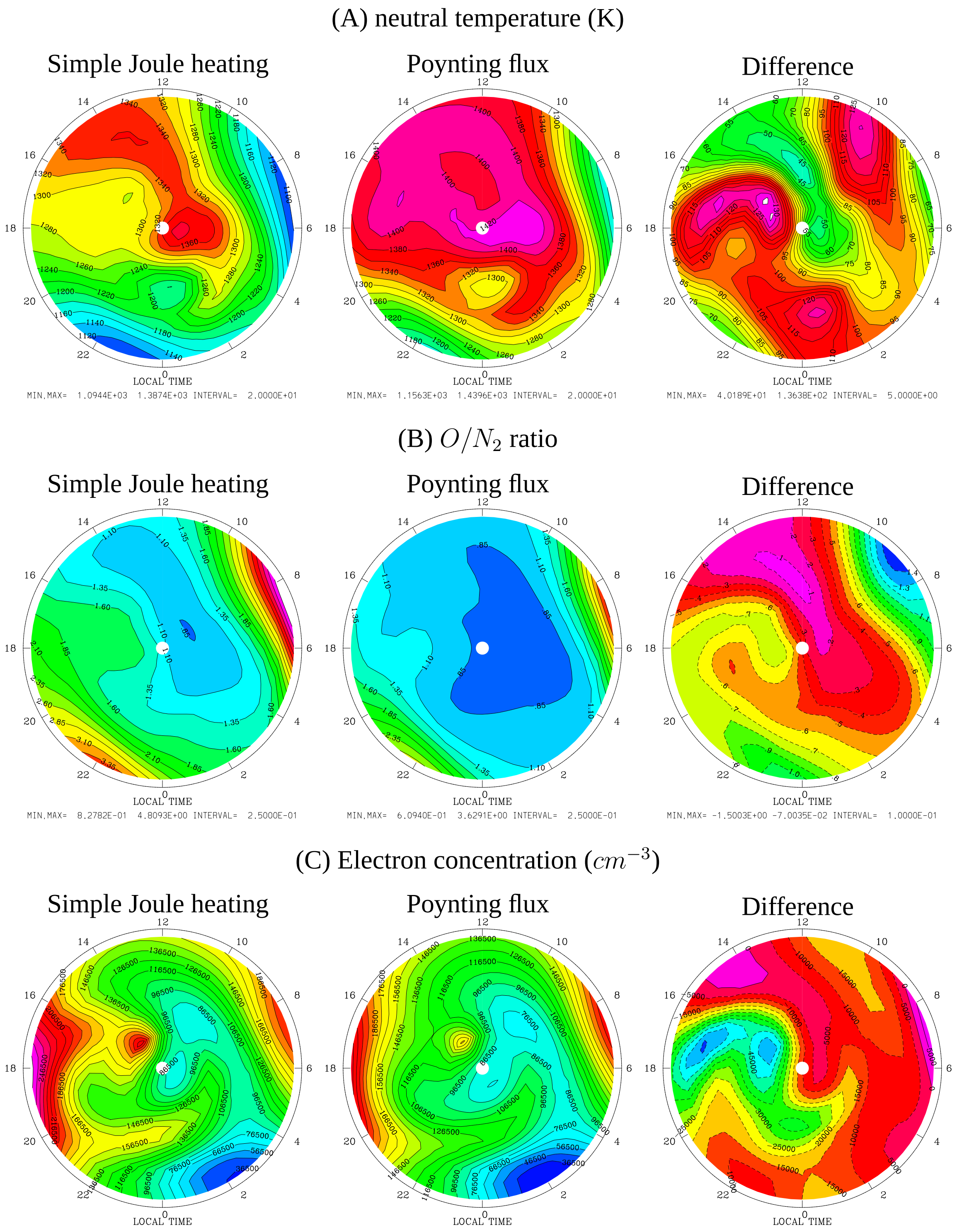

Figure 4. Same as Figure 2, but (A) for neutral temperature (K), (B) for composition (O/N^2 ratio) and (C) for electron density (cm^{-3}).

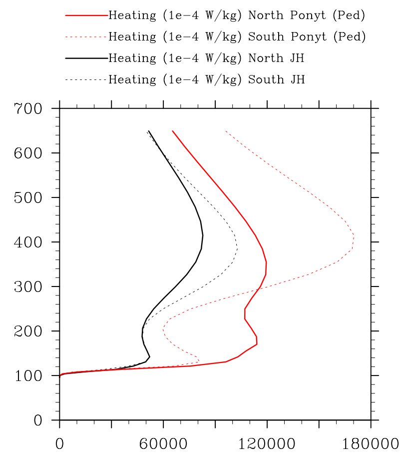

Figure 5. Altitude profile of the polar average (poleward 40° for the northern hemisphere and -40° for the southern hemisphere) heating per unit mass ($erg/g/s[= 10^{-4} W/kg]$) for the simple Joule heating case (black lines) and Poynting flux case (red lines). The solid lines represent the northern (summer) hemisphere and the dash lines represent the southern (winter) hemisphere.

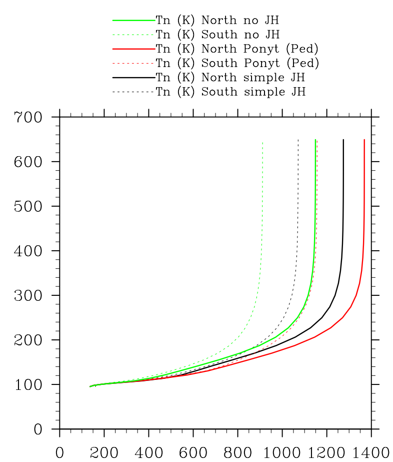

Figure 6. Altitude profile of the polar average (poleward 40° for the northern hemisphere and -40° for the southern hemisphere) neutral temperature (K) for the case without Joule heating in the polar region (blue lines), the simple Joule heating case (black lines) and Poynting flux case (red lines). The solid lines represent the northern (summer) hemisphere and the dash lines represent the southern (winter) hemisphere.

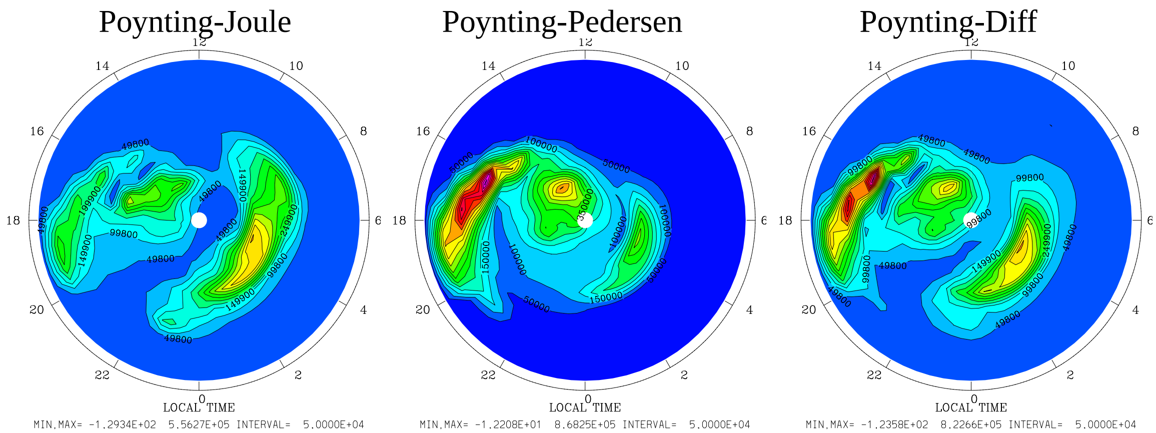

Figure 7. heating per unit mass ($erg/g/s[= 10^{-4}W/kg]$) at 400 km altitude in the northern (summer) hemisphere for the (left) Poynting-Joule, (middle) Poynting-Pedersen and (right) Poynting-Diff cases.

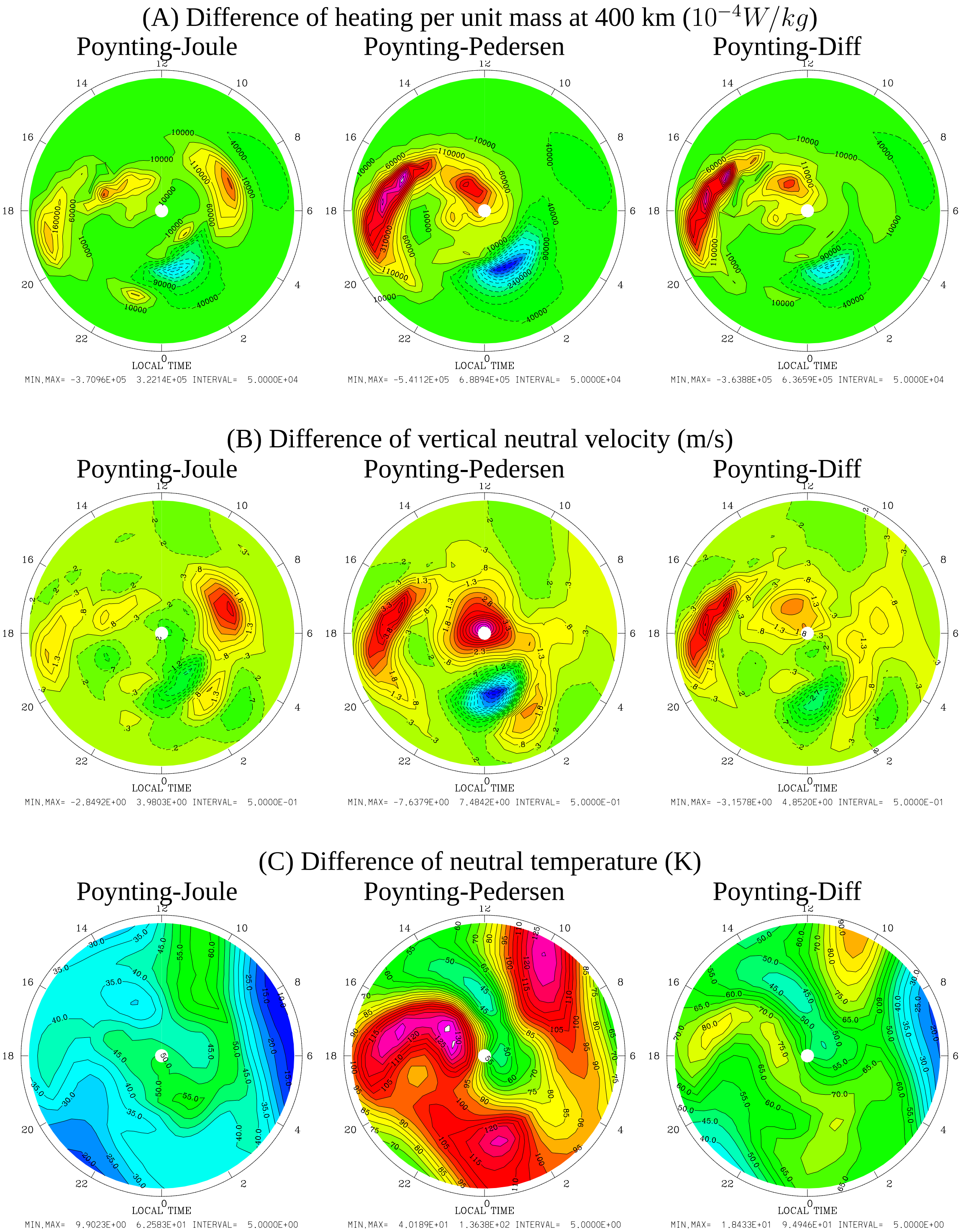

Figure 8. The difference of (A) heating per unit mass ($10^{-4}W/kg$), (B) vertical neutral velocity (m/s) and (C) neutral temperature (K) at 400 km altitude in the northern (summer) hemisphere when compared to the simple Joule heating case. The right column shows the Poynting-Joule case, the middle column shows the Poynting-Pedersen case and the right column shows the Poynting-Diff case.

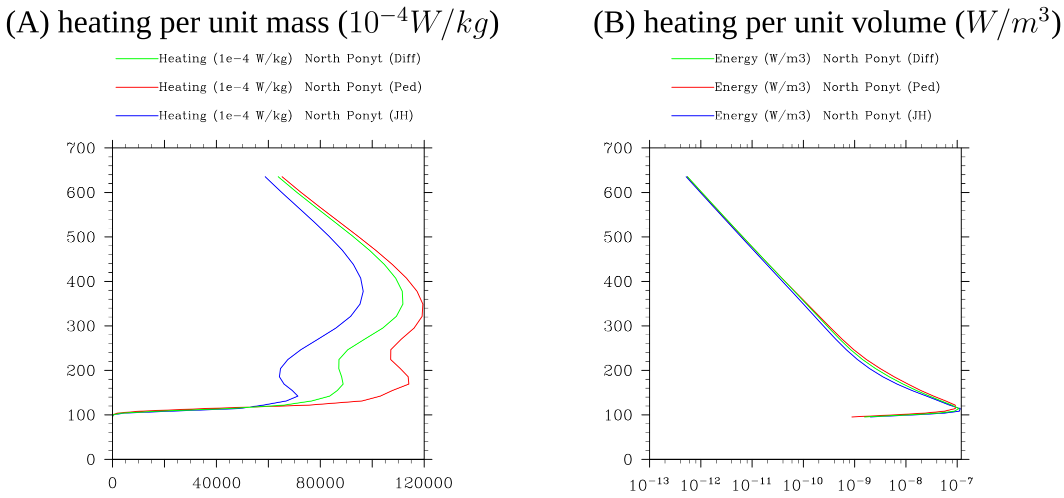

Figure 9. Same as Figure 5, but blue lines for the Poynt (JH) case, red lines for the Poynt (Ped) case and the green lines for the Poynt (Diff) case.

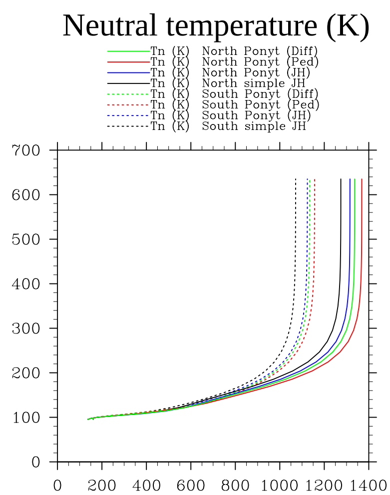

Figure 10. Same as Figure 6, but black lines for the simple Joule heating case, blue lines for the Poynting-Joule case, red lines for the Poynting-Pedersen case and the green lines for the Poynting-Diff case.